

# Journal Pre-proof

Low-frequency electrokinetics in a periodic pillar array for particle separation

Víctor Calero, Raúl Fernández-Mateo, Hywel Morgan, Pablo García-Sánchez and Antonio Ramos

PII: S0021-9673(23)00465-X  
DOI: <https://doi.org/10.1016/j.chroma.2023.464240>  
Reference: CHROMA 464240

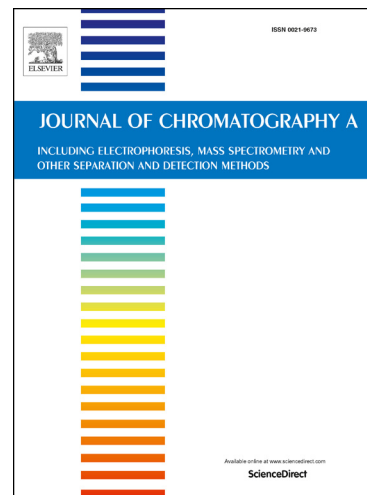
To appear in: *Journal of Chromatography A*

Received date: 18 April 2023  
Revised date: 18 July 2023  
Accepted date: 23 July 2023

Please cite this article as: V. Calero, R. Fernández-Mateo, H. Morgan et al., Low-frequency electrokinetics in a periodic pillar array for particle separation, *Journal of Chromatography A*, 464240, doi: <https://doi.org/10.1016/j.chroma.2023.464240>.

This is a PDF file of an article that has undergone enhancements after acceptance, such as the addition of a cover page and metadata, and formatting for readability, but it is not yet the definitive version of record. This version will undergo additional copyediting, typesetting and review before it is published in its final form, but we are providing this version to give early visibility of the article. Please note that, during the production process, errors may be discovered which could affect the content, and all legal disclaimers that apply to the journal pertain.

© 2023 Published by Elsevier.



## Highlights

- Low frequency electrokinetics improves Deterministic Lateral Displacement separation.
- CPEO driven wall-repulsion plays a major role in this mechanism.
- Combination of Electrophoresis and CPEO fully explains the low frequency separation.
- The mechanism of Electrokinetic biased DLD separation has been fully characterized.
- This model enables numerical optimization of future electrokinetic DLD devices.

Journal Pre-proof

# Low-frequency electrokinetics in a periodic pillar array for particle separation

Víctor Calero,<sup>1,2</sup> Raúl Fernández-Mateo,<sup>3</sup> Hywel Morgan,<sup>3</sup> Pablo García-Sánchez,<sup>1,\*</sup> and Antonio Ramos<sup>1</sup>

<sup>1</sup>*Depto. Electrónica y Electromagnetismo. Facultad de Física. Universidad de Sevilla. Avda. Reina Mercedes s/n, 41012. Sevilla (Spain).*

<sup>2</sup>*International Iberian Nanotechnology Laboratory (INL), Braga 4715-330, Portugal.*

<sup>3</sup>*School of Electronics and Computer Science, University of Southampton, Southampton SO17 1BJ, United Kingdom.*

Deterministic Lateral Displacement (DLD) exploits periodic arrays of pillars inside microfluidic channels for high-precision sorting of micro- and nano-particles. Previously we demonstrated how DLD separation can be significantly improved by the addition of AC electrokinetic forces, increasing the tunability of the technique and expanding the range of applications. At high frequencies of the electric field (>1kHz) the behaviour of such systems is dominated by Dielectrophoresis (DEP), whereas at low frequencies the particle behaviour is much richer and more complex. In this article, we present a detailed numerical analysis of the mechanisms governing particle motion in a DLD micropillar array in the presence of a low-frequency AC electric field. We show how a combination of Electrophoresis (EP) and Concentration-Polarisation Electroosmosis (CPEO) driven wall-particle repulsion account for the observed experimental behaviour of particles, and demonstrate how this complete model can predict conditions that lead to electrically induced deviation of particles much smaller than the critical size of the DLD array.

## I. INTRODUCTION

Over the last decades, there has been an increased interest in the development of microfluidic particle separation techniques. Low-volume high-precision fractionation methods are important for the development of devices capable of performing full analytical processes on a single platform. Examples include the isolation, detection and monitoring of a wide range of bioparticles (such as circulating tumour cells (CTCs), bacteria or extracellular vesicles [1–4]) from complex samples that ultimately enable early diagnosis and monitoring of disease.

Deterministic Lateral Displacement (DLD) is a promising microfluidic separation approach that delivers high-resolution continuous-flow size-based separation of particles over a wide range of sizes, from nanoparticles to cells that are tens of micrometers in size [5, 6]. DLD devices take advantage of laminar flow on the microscale to sort particles in a deterministic way based on a specific geometry of an array of micro-pillars. In the DLD geometry each row of posts is displaced a given distance ( $\Delta\lambda$ ) from the previous, defining a periodicity  $P$  given by:

$$P = \frac{\lambda}{\Delta\lambda} \quad (1)$$

where  $\lambda$  is the distance between consecutive rows of pillars. Figure 1 shows a diagram of the typical DLD pillar array geometry and the physical mechanism responsible for size-based separation. The shift in the consecutive rows gives rise to a separatrix streamline which divides the fluid flow into portions passing above and below the

next post. If a particle is bigger than the minimum distance from the separatrix to the nearest post, upon interaction with this post, it will be displaced towards the portion of fluid passing above the following post. As a result, particles follow the deviation angle defined by the array geometry ( $\theta_D = \arctan(1/P)$ ), bumping on the posts and displacing laterally (dark particles in Figure 1). If on the contrary, the particle is smaller than the distance from the separatrix to the post, it is not displaced by the posts and will remain in the fluid passing below the next post, following an overall straight trajectory with zero net lateral displacement, zigzagging around the pillars (light particles in Figure 1). The critical diameter ( $D_c$ ) is thus defined as the diameter above which the particles follow deviating trajectories and is therefore determined by the width of the separatrix near the posts. For a more detailed description of this mechanism see [7].

Since first reported by Huang *et al.* [8], DLD separation has been extensively studied and enhanced. A particularly interesting and promising approach consists of coupling DLD with external fields, turning passive DLD size-based separation into active and tunable sorting that can target additional physical properties of the particles rather than size. Amongst the many options, coupling DLD with electric fields has proven to be a very useful approach with a rich number of physical mechanisms leading to enhanced particle separation. This approach was first reported by Beech *et al.* [9], applying an AC electric field along the DLD channels in the direction parallel to the fluid flow. They showed tunable separation of 3  $\mu\text{m}$  and 5  $\mu\text{m}$  diameter particles inside a DLD device with 6  $\mu\text{m}$  critical diameter, and attributed the induced deviation to Dielectrophoresis (DEP). Later [10] they showed that the particle behaviour is much richer than first claimed and explored how the deviation depended on the suspending electrolyte conductivity, the particle charge and the electric field frequency.

\* Corresponding author: pablogarcia@us.es

In recent articles, we explored the induced deviation of particles smaller than the  $D_c$  when an AC electric field is applied orthogonal to the fluid flow [11, 12]. We first characterised the particle behaviour and induced separation of 500 nm, 1  $\mu\text{m}$  and 3  $\mu\text{m}$  in a DLD with a  $D_c$  of 6.3  $\mu\text{m}$  as a function of the electric field frequency. Two different regimes were identified. At high frequencies ( $> 1$  kHz), particle behaviour was dominated by DEP whereas at low frequencies other mechanisms came into play. The scaling laws governing the electrokinetic induced behaviour at both, high and low frequencies were explored. It was demonstrated that negative DEP (nDEP) drove the separation at high frequencies and good agreement was found between the experimental results and numerical simulations. At low frequencies dependence of the separation was characterised as a function of the magnitude of the electric field, particle size and fluid velocity. A full theoretical model was not available at the time to account for the observations.

In this paper, we present a thorough and detailed numerical study of the low-frequency AC electrokinetic behaviour of the particles within a DLD pillar array. The model considers the low-frequency oscillating Electrophoresis (EP) along the electric field lines around the pillars together with wall-particle repulsion that occurs during EP [13–15]. We recently described the latter mechanism as driven by stationary electroosmotic (EO) flows around the particles due to Concentration-Polarization (CP) of the electrolyte surrounding the particle, termed CPEO [16, 17]. The results are in excellent agreement with the observed experimental trends. This last analysis completes the understanding of the electrokinetic behaviour of particles inside the DLD devices and provides a full theoretical framework to explain the electrokinetic biased DLD particle separation.

## II. THEORY

### A. High frequency regime ( $f \gtrsim 1$ kHz)

Figure 2 shows a diagram of the two different regimes of AC electrokinetic induced deviation in a DLD channel for high and low frequencies of the electric field. At high frequencies, the DEP force dominates the particle behaviour. The force arises from the spatial gradient in the electric field due to the insulating pillars (see Figure 2a). The time average DEP acting on a particle subjected to an AC field [18, 19]  $\mathbf{E} = \text{Re}[\mathbf{E}_0(\mathbf{r})e^{i\omega t}]$  is given by:

$$\mathbf{F}_{\text{DEP}} = \pi a^3 \varepsilon \text{Re}[f_{CM}] \nabla |\mathbf{E}_0|^2 \quad (2)$$

where  $a$  is the particle radius,  $\varepsilon$  the medium permittivity,  $f_{CM}$  is a complex parameter known as the Clausius-Mossotti factor and  $\text{Re}[\dots]$  denotes the real part of the function between brackets. The parameter  $f_{CM}$  relates

the polarisabilities of the particle and the surrounding medium. When a particle is less polarisable than the medium,  $\text{Re}[f_{CM}] < 0$  it experiences nDEP, i.e. it is repelled from high electric field gradients. When this occurs in the DLD shown in Figure 2a, the particles are repelled from the downstream gaps between the posts. If the nDEP repulsion is strong enough to disrupt the particle trajectories and make them cross the separatrix streamline, the particles are therefore prevented from zigzagging between the posts and are forced to follow a deviating trajectory. Under the influence of a DEP force and a fluid velocity field  $\mathbf{v}_f$ , the particle velocity  $\mathbf{u}$  is given by:

$$\mathbf{u} = \mathbf{v}_f + \mathbf{u}_{\text{DEP}} \quad (3)$$

with  $\mathbf{u}_{\text{DEP}} = \frac{a^2 \varepsilon \text{Re}[f_{CM}]}{6\eta} \nabla |\mathbf{E}_0|^2$ , where  $\eta$  is the dynamic viscosity of the fluid. Following the analysis in Calero *et al.* [12], a dimensionless expression of equation (3) can be derived using the post radius  $R$ , a typical fluid velocity  $U$ , and a typical electric field magnitude  $E_0$ :

$$\tilde{\mathbf{u}} = \tilde{\mathbf{v}}_f + \text{sgn}(\text{Re}[\tilde{f}_{CM}]) N \tilde{\nabla} |\tilde{\mathbf{E}}_0|^2 \quad (4)$$

where the tilde indicates dimensionless magnitudes. In this equation, the dimensionless parameter  $N = \frac{\varepsilon E_0^2 a^2}{6\eta R U} |\text{Re}[f_{CM}]|$  quantifies the relative contribution of the DEP force to the net particle velocity, and therefore the deviation induced by this force scales with the magnitude of this parameter.

### B. Low frequency regime ( $f \lesssim 1$ kHz)

For frequencies below  $\sim 1$  kHz, other forces come into play. Although the oscillating EP has a zero time-average displacement, it leads to an oscillation of the particle along the electric field lines (see Figure 2b), with a velocity  $\mathbf{u}_{\text{ep}}$  given by the Helmholtz-Smoluchowski equation:

$$\mathbf{u}_{\text{EP}} = \frac{\varepsilon \zeta}{\eta} \mathbf{E} \quad (5)$$

where  $\zeta$  is the zeta potential of the particle [20]. We hypothesise that this oscillation leads to a pronounced interaction between the walls of the DLD posts and the finite-sized rigid particles as they flow along the microchannels, creating an induced deflection.

However, low-frequency EP is not the only phenomenon that is present at low frequencies. We recently reported the presence of Concentration-Polarization Electroosmotic (CPEO) flows around charged dielectric particles subjected to low-frequency AC electric fields [16]. The particle surface conductance leads to a perturbation in the local electrolyte concentration, and therefore in the electroosmotic slip velocity at the particle surface, creating a stationary quadrupolar flow pattern, as

177 shown in Figure 3a. The fluid velocity field was derived  
178 by Gamayunov *et al.* [21] and is given by:

$$\mathbf{v}_{\text{CPEO}} = v_0 \left( \frac{(1 - (r/a)^2)(1 + 3 \cos 2\theta)}{2(r/a)^4} \hat{r} + \frac{\sin 2\theta}{(r/a)^4} \hat{\theta} \right) \quad (6)$$

179 where  $r$  is the distance to the particle centre and  $\theta$  is the  
180 angle with respect to the flow symmetry axis, which coin-  
181 cides with the direction of the applied electric field. The  
182 parameter  $v_0$  is the maximum slip velocity at the parti-  
183 cle surfaces and scales with the electric field magnitude  
184 squared [16],  $v_0 = \frac{\varepsilon a E_0^2}{\eta} \tilde{v}_0(f, \zeta, a, \dots)$ . As a result, the  
185 CPEO flows have a non-zero time average velocity with  
186 a quadratic dependence on the electric field magnitude.  
187 Their magnitude decreases with electrolyte conductivity  
188 and AC field frequency and increases with the particle  
189 surface charge. A complete theoretical description of this  
190 mechanism can be found in [16].

191 In a previous publication [15] we demonstrated that  
192 CPEO flow is the dominant mechanism that creates the  
193 observed particle-wall repulsion during Electrophoresis of  
194 charged dielectric particles. Our results show that the  
195 hydrodynamic interaction due to CPEO flows overcomes  
196 the DEP forces in the low frequency regime and that the  
197 latter can only explain the observed particle-wall sepa-  
198 ration at high frequencies. In the presence of a low fre-  
199 quency AC electric field and with the particle situated in  
200 the vicinity of a wall, the CPEO flow patterns become  
201 distorted, as shown in Figure 3b. This hydrodynamic in-  
202 teraction gives rise to a net particle velocity with respect  
203 to the nearby wall which can be calculated following the  
204 method of reflections [22]. For the case of an electric  
205 field parallel to the wall, there is a net particle repulsion  
206 perpendicular to the wall given by [23, 24]:

$$\mathbf{u}_{\text{rep}} = v_0 \frac{3a^2}{8h^2} \hat{z} \quad (7)$$

207 where  $h$  is the distance from the particle center to the  
208 wall and  $\hat{z}$  the unit vector which is perpendicular to the  
209 wall. The constant  $v_0$  is the CPEO slip velocity at the  
210 surface of the particle [16]. This is the leading-order term  
211 in the method of reflections for small values of  $a/h$ . A  
212 similar analysis can be used to predict the particle veloc-  
213 ity perpendicular to the wall for the case of an electric  
214 field perpendicular to the wall. In this case, the CPEO  
215 flow leads to wall-particle attraction with a velocity given  
216 by [24]:

$$\mathbf{u}_{\text{at}} = -v_0 \frac{3a^2}{4h^2} \hat{z} \quad (8)$$

217 Smart and Leighton [24] also showed that, when the  
218 field is at an angle to the surface of the flat wall ( $0 < \theta$   
219  $< \pi/2$ ), there is an extra component to the particle  
220 velocity, that is tangential to the wall given by:

$$\mathbf{u}_{\text{tan}} = -v_0 \frac{3a^2}{4h^2} \sin \varphi \cos \varphi \hat{x} \quad (9)$$

A detailed derivation of these equations can be found in  
the supplementary material.

In this paper, we describe the role of this mechanism in  
a DLD array as particles are repelled from the posts. We  
hypothesize that the CPEO particle-wall repulsion plays  
a mayor role in the low-frequency electrokinetic-induced  
deviation. Every time a particle approaches a DLD pillar,  
the hydrodynamic interaction leads to particle repulsion  
from the pillar. If this repulsion is strong enough, then  
particles are forced to switch from a zigzagging trajectory  
to the displacement mode, following the array deviation  
angle (see Figure 3c).

### III. NUMERICAL METHODS

#### A. High frequency regime simulations

At high electric field frequencies, the only forces acting  
on the particles are the hydrodynamic drag force from the  
net fluid flow along the microfluidic channels and DEP.  
To simulate this situation we followed the exact same  
methods previously described by Calero *et al.* [12]. The  
spatial distribution of the electric field and fluid flow ve-  
locity is first calculated inside a DLD unit cell (see Fig-  
ure 4a) using Finite Element Analysis and the software  
COMSOL Multiphysics v5.4. To calculate the fluid flow,  
the 2D Stokes equation ( $Re \sim 10^{-3}$ ) was solved with  
periodic boundary conditions in the perpendicular and  
longitudinal directions, enforcing a zero net velocity in  
the direction perpendicular to the flow and mean fluid  
velocity magnitude of  $U = 100 \mu\text{m/s}$  in the longitudinal  
direction. A no-slip boundary condition was used at the  
surface of the posts. The electric field  $\mathbf{E}$  was calculated  
from the perturbation  $\mathbf{E}'$  of a uniform field  $E_0 \hat{y}$ . For the  
case of an electric field in the direction  $y$  (perpendicular  
to the fluid flow):

$$\mathbf{E} = \mathbf{E}' + E_0 \hat{y} \rightarrow \phi = \phi' - E_0 y \quad (10)$$

Thus, to calculate  $\mathbf{E}'$  the Laplace equation was solved  
for the electrical potential  $\phi'$  with periodic boundary con-  
ditions at the boundaries of the unit cell. To model the  
pillars as insulators the following condition was used at  
the surface of the posts:

$$\frac{\partial \phi}{\partial n} = 0 \rightarrow \frac{\partial \phi'}{\partial n} = E_0 n_y \quad (11)$$

where  $n_y$  is the  $y$ -component of a unit vector normal to  
the boundary.

Figure 4a shows the spatial dependence of the fluid  
velocity and electric field magnitude in the DLD unit

cell. The trajectories of more than 2000 particles inside a DLD unit cell are simulated for different initial positions equally distributed and covering the entire possible range, with the velocity given by equation (3).

The initial and final positions (as defined in Figure 4a.i) are related by a transfer function which can then be used to calculate, using linear interpolation, the final position of any particle entering the unit cell for any value of initial position [12, 25]. The transfer function will thus depend on the ratio between the fluid drag force and the DEP force and can be used to estimate the deviation angle after a particle crosses a large number of unit cells. In every iteration, a particle in deviation mode exits the unit cell at the same distance from the nearest post at which it entered. This is then reflected in the transfer function by crossing the line of slope 1 that passes through the origin, i.e. in the trajectory across the unit cell the initial and final positions (as defined in Figure 4a.i) are equal.

In this study we used parameters that enabled comparison with the experimental results [12]:  $U = 100 \mu\text{m/s}$ ,  $\text{Re}[\tilde{f}_{CM}] = -0.5$ ,  $a = 0.5, 1.5 \mu\text{m}$  and  $|\mathbf{E}_0| < 80 \text{kV/m}$  and with a symmetric DLD geometry with  $D_p = \lambda/2$  and  $P = 18$  ( $\theta = 3.18^\circ$ ). The particle-wall interaction was modeled as a non-elastic hard wall collision as described by Kim *et al.* [25] and in our previous work [12]. Briefly, we considered an exclusion zone of one particle radius around the posts. Thus particles with an initial/final position closer than  $a$  to a post were considered to enter/exit the unit cell at a distance  $a$  from that post. In the transfer function, this translates into removing the prohibited initial and final (exit) positions from this function [12].

## B. Low-frequency regime simulations

In the low-frequency regime, the approach used for high frequencies is not valid because of the significant electrophoretic oscillation of particles. This introduces an extra degree of complexity through the addition of a new parameter, the phase of the electric field. This is because the phase of the field with which the particle enters the unit cell differs from the exiting phase, depending on the time the particle takes to cover the distance of the unit cell. This adds an extra dimension to the numerical simulations and turns the 1D-1D transfer function into a 2D-2D function. The supplementary material includes a diagram of the workflow followed for the simulation procedure for both cases (high and low frequencies).

To circumvent this complexity, a different approach was taken by simply simulating the trajectories of a single particle after it has crossed a large number of unit cells. To realise this the electric and fluid fields were exported to MATLAB R2022b and the particle trajectories were calculated across a large number of unit cells (360 unit cells, i.e. 20 periods of the DLD array), until the

trajectory converged into either a zig-zag or displacement mode. The components of the particle velocity are:

$$\mathbf{u} = \mathbf{v}_f + \mathbf{u}_{EP} + \mathbf{u}_{rep} + \mathbf{u}_{at} \quad (12)$$

For simplicity the tangential component  $\mathbf{u}_{tan}$  (given by equation (9)) was not considered in the simulations since this component is much smaller than the electrophoretic velocity ( $\mathbf{u}_{ep} \gg \mathbf{u}_{tan}$ ). The EP velocity  $\mathbf{u}_{ep}$  is given by equation (5), which for an oscillating field with angular frequency  $\omega$  and phase  $\varphi$ ,  $\mathbf{E} = \mathbf{E}_0 \cos(\omega t + \varphi)$ , produces an oscillating motion along the electric field lines, only relevant for low values of  $\omega$ . The values for  $\zeta$  were measured experimentally and used as input to the model:  $\zeta = -70 \text{ mV}$  and  $\zeta = -78 \text{ mV}$  for the  $1 \mu\text{m}$  and  $3 \mu\text{m}$  diameter particles, respectively. Since in this case the electric field is neither tangential nor perpendicular to the pillar wall, to calculate the contribution of the CPEO hydrodynamic interaction  $\mathbf{u}_{rep}$  and  $\mathbf{u}_{at}$  were calculated at each point of the unit cell as:

$$\mathbf{u}_{rep} = v_0 \frac{3a^2}{8h^2} \frac{|E_t|^2}{|E_0|^2} \hat{n}, \quad (13)$$

$$\mathbf{u}_{at} = -v_0 \frac{3a^2}{4h^2} \frac{|E_n|^2}{|E_0|^2} \hat{n}, \quad (14)$$

where  $E_t$  and  $E_n$  are, respectively the tangential and normal components of the electric field to the pillar wall at the particle position and  $\hat{n}$  a unit vector perpendicular to the wall [26]. The value for  $v_0$  is the only input to the model and was estimated experimentally following the methods described by Fernandez-Mateo *et al.* [15], where the wall-repulsion was measured along a straight channel with the electric field applied parallel to the fluid flow. This was done in conditions that allowed comparison to published experimental data [12] (at an electrolyte conductivity of  $2.8 \text{ mS/m}$ , an electric field of  $50 \text{ Hz}$  and  $60 \text{ kV/m}$ , and particle diameters of  $1$  and  $3 \mu\text{m}$ ):  $v_0 = (109.4 \pm 18.6) \mu\text{m/s}$  for  $1 \mu\text{m}$  particles and  $v_0 = (324.5 \pm 25.0) \mu\text{m/s}$  for  $3 \mu\text{m}$  particles. In order to estimate  $v_0$  for other electric field magnitudes, the measurements at  $60 \text{ kV/m}$  were used together with the quadratic dependence with  $|E|$  predicted by the CPEO model [16]. This model also allows to predict a theoretical value for  $v_0$  from the particle/medium properties and the electric field magnitude and frequency, but measuring  $v_0$  experimentally allows a more accurate comparison with our numerical model.

Finally, the particle-wall interaction was modelled as a hard-wall inelastic collision. At each time step, if a particle approached the post boundary at a distance smaller than a particle radius, the particle position was corrected the same distance in the direction perpendicular to the wall. An example of this correction is given in Figure 4b.

A typical trajectory of a  $3\ \mu\text{m}$  particle across a DLD unit cell under the influence of a low-frequency electric field ( $E_0 = 20\ \text{kV/m}$  and  $f = 50\ \text{Hz}$ ), i.e. EP and CPEO wall interaction is shown in Figure 4c.

With this model we are replicating the experimental design described in Calero et al. [12] where the devices were pretreated with a surfactant (Pluronic F-127) to avoid particle adhesion and minimize electroosmotic flow [27–29]. Consequently, in the simulations the low frequency oscillation are solely caused by electrophoresis. Also note that CPEO flows around the insulating posts are not considered ([12, 30]) due to the fact that the post diameter is larger than the height of the microchannels. Since the upper and lower walls are very close, the no-slip condition significantly reduces the magnitude of these flows. Finally, for simplicity, we have assumed in this regime that the DEP contribution is negligible with respect to the contributions of EP and CPEO. This assumption is supported by experimental data where the low-frequency deviation is demonstrated regardless of the DEP behavior of the particles: induced deviation was observed not only for nDEP particles but, also, for particles with positive DEP (pDEP) or with  $\text{Re}[\tilde{f}_{CM}] \sim 0$ . Numerical data in the results section validate this simplification.

## IV. RESULTS

### A. Simulation results and comparison with experimental data

To test the model, the dependence of the deviation angle for  $1\ \mu\text{m}$  and  $3\ \mu\text{m}$  diameter rigid spheres was analysed as a function of the applied electric field magnitude, at high and low frequencies for an electric field applied perpendicular to the fluid flow. We then compared the results with the experimental data previously reported [12]. The results are summarised in Figure 5. The deviation angle is directly calculated from the net lateral displacement given by the simulations, and is plotted against the ratio  $E_0 a / \sqrt{U}$ , to enable a direct comparison between all data sets (with different values of  $U$  and particle sizes). This is valid since it is the ratio between the quadratic electric forces and the hydrodynamic drag from the fluid flow. This leads to an overlapping set of curves for the nDEP induced deviation. Note that the simulations at high frequencies assume  $\text{Re}[\tilde{f}_{CM}] = -0.5$ , i.e. the nDEP magnitude is maximum and therefore nDEP induced deviation is also maximum. For the experimental conditions at which the deviation and the parameter  $v_0$  were measured, the nDEP is even weaker for the  $3\ \mu\text{m}$  particles with  $\text{Re}[\tilde{f}_{CM}] = -0.21$  or is even positive DEP for the  $1\ \mu\text{m}$  particles with  $\text{Re}[\tilde{f}_{CM}] = 0.12$ .

The figure shows that at low frequencies the results from the model (including contributions from EP oscillation and CPEO) match the experimental trends. It

predicts a clear difference in the critical electric field, i.e. the value of  $|E_0|$  at which the particles switch to the displacement mode, for the two different particle sizes as observed experimentally. Furthermore, the model predicts a critical field lower than that given by the nDEP mechanism and much closer to the experimental results. This is particularly noticeable for the smallest particle size. Importantly, experiments show a much smoother transition from zero lateral displacement to the maximum deviation angle, mainly for the smaller particles. This is not predicted by the simulations, which show an abrupt transition between displacement or zig-zag. This sharp transition is expected from a fully deterministic behaviour of the particles. The smoothness observed experimentally is attributed to experimental artifacts not accounted for in the simulations, mostly the non-uniformity of the electric field magnitude across the channel caused by changes in the local conductivity near the electrodes[31].

Although the deviation angle defined by the DLD array is equal in both experiments and simulations, there is an observed difference in the maximum value of the deviation angle. This is simply due to the specific design of the experimental DLD devices (explained in [12]). The devices have a region near the electrode with zero pillar array offset where fully deflected particles concentrate. Particles in a displacement trajectory reach this region before they arrive at the end of the channel, and travel in a straight line with zero deviation. Since the experimental deviation angle is estimated from the total displacement at the end of the channel and the channel length, this leads to a smaller angle than that defined by the array geometry.

### B. Low frequency behaviour: contributions of EP and CPEO

The numerical model was then used to analyse the contribution of the CPEO particle-wall interaction to the deviation with a low frequency electric field perpendicular to the flow. For this purpose, particle trajectories were simulated taking into account solely the influence of the EP oscillation or the influence of combination of EP and CPEO. Figure 6 summarises the results for the deviation of  $1\ \mu\text{m}$  and  $3\ \mu\text{m}$  particles at  $50\ \text{Hz}$  and a  $v_0$  measured at this frequency and  $2.8\ \text{mS/m}$ . It shows that the EP oscillation alone can induce deviation of particles via inelastic collision with the pillar walls. We hypothesise that the collisions limits the oscillating motion towards the posts giving a non-zero time average lateral displacement that is magnified after interaction with several posts. The symmetry of this mechanism is broken by the tilt angle of the DLD array, leading to a preferential direction in the post-particle interaction driven by the EP oscillation.

However, as shown in Figure 6, the critical field is significantly reduced when the CPEO wall interaction is included in the simulations. Importantly, there was no

468 deviation when only the CPEO wall-interaction is con-523  
 469 sidered (ignoring the EP oscillation) for any of the two524  
 470 particles sizes, in the range of field amplitudes explored.525  
 471 Figure 6a shows the low frequency deviation for two dif-526  
 472 ferent particle sizes, demonstrating that the reduction527  
 473 in the critical field is more noticeable for the smallest528  
 474 particles. Figure 6b shows how the deviation of the 3529  
 475  $\mu\text{m}$  diameter spheres depends on the frequency of the530  
 476 applied electric field. It shows that, as the frequency in-531  
 477 creases, the influence of the CPEO interaction becomes532  
 478 more prominent. At 50 Hz, the addition of CPEO de-533  
 479 creases the critical field magnitude by  $\sim 5\%$  whereas for534  
 480 167 Hz the reduction is more than 30%. This implies535  
 481 that as frequency increases, the contribution of the EP  
 482 oscillations decreases faster than the CPEO wall interac-  
 483 tion.

484 Figure 7 shows an example of how this mechanism536  
 485 works. It shows the trajectory of a 1  $\mu\text{m}$  diameter rigid537  
 486 sphere in a DLD array under the influence of a 50 Hz538  
 487 field perpendicular to the flow for: (a) the EP force, (b)539  
 488 the CPEO wall-interaction and (c) combination of both.540  
 489 These simulations were done at a field of 43 kV/m, cor-541  
 490 responding to the regime where the EP oscillation alone542  
 491 does not induce deviation, but only when combined with543  
 492 CPEO. Figure 7a depicts how, when only the EP force544  
 493 is considered, the particles barely interact with the posts545  
 494 because of the distortion of the electric field lines around546  
 495 the insulating posts. When the CPEO wall interaction is547  
 496 the only mechanism (Figure 7b), particles only pass near548  
 497 the posts for a small portion of their trajectories. Since549  
 498 the CPEO decays with distance to the wall squared, this550  
 499 interaction does not lead to a large change in the par-551  
 500 ticle trajectory. When both mechanisms are combined552  
 501 (Figure 7c), the particle oscillations along the field lines553  
 502 drives the particles near the post walls, maximising the554  
 503 effect of the CPEO particle-wall interaction leading to the  
 504 induced particle deviation. These results lead to the con-  
 505 clusion that only when both mechanisms are combined,  
 506 there is an accurate prediction of the observed experi-555  
 507 mental trends. Thus there is a non-linear dependence of556  
 508 the induced deviation with the electric field magnitude,557  
 509 a decline with the electric field frequency and the elec-558  
 510 trolyte conductivity and the lack of a direct relationship559  
 511 between the oscillation amplitude and the induced devi-560  
 512 ation.

### 513 C. Comparison between a parallel and a 514 perpendicular field

515 Finally the particle trajectories were examined with567  
 516 the electric field applied parallel to the fluid flow. This568  
 517 configuration has been experimentally characterised by569  
 518 Tegenfeldt *et al.* [9, 10, 32]. They found very similar570  
 519 trends with nDEP dominating at high frequencies and/or571  
 520 high medium conductivities; the high frequency devia-572  
 521 tion can be fully explained by DEP. However, deviation573  
 522 at low frequencies is different, with the effect decreas-574

ing with the field frequency and electrolyte conductivity.  
 Interestingly, they also showed that the particle surface  
 charge was directly linked to the low frequency induced  
 deviation [10]. Under the same conditions, particles with  
 a higher surface charge had a reduced critical electric  
 field magnitude, i.e. they deviated for lower values of  
 field strength. This matches the hypothesis that the low  
 frequency deviation is dominated by a combination of  
 CPEO and EP oscillation, since both mechanisms are  
 stronger for a higher surface charge density. Also, in this  
 case, the EP oscillation occurs in the direction of the fluid  
 flow (along the field lines), so that this mechanism alone  
 could not lead to an increased wall-particle interaction.

The simulations show that when the field is applied in  
 the direction of fluid flow, there is no induced deviation  
 when any of the two mechanisms, CPEO wall interac-  
 tion or EP oscillation, is considered independently. Only  
 when the two are combined does the electric field force  
 the particles to switch to the displacement mode. In  
 contrast to the perpendicular field, with the field parallel  
 to the fluid flow, the EP oscillation takes place in the  
 direction of the fluid streamlines and so does the inelas-  
 tic post-particle interaction. As a result, the oscillations  
 alone cannot produce the net displacement required to  
 push particles across the separatrix streamline. Similar  
 to the perpendicular case, when the CPEO acts inde-  
 pendently, particles only spend a small fraction of time  
 near the posts, so that the effects of the CPEO wall in-  
 teraction are largely reduced. Only when the oscillating  
 trajectories drive the particles back and forth near the  
 post wall, does the CPEO effect accumulate forcing the  
 particles to deviate.

Figure 8 shows the simulation results at 50 Hz with  
 the field applied in the direction of the fluid flow (as a  
 function of electric field magnitude). The figure shows  
 a comparison with the maximum nDEP induced devia-  
 tion. For the 1  $\mu\text{m}$  particles, there is a negligible dif-  
 ference between the critical field magnitude given by the  
 nDEP mechanism and the low frequency induced devi-  
 ation. However, for the bigger particles of 3  $\mu\text{m}$ , there  
 is a significant reduction in critical field magnitude for  
 the low frequency mechanism. This figure also provides  
 a comparison between the predicted low frequency devi-  
 ation for an electric field applied perpendicular ( $\perp$ ) and  
 parallel ( $\parallel$ ) to the fluid flow. The predicted deviation of  
 the 3  $\mu\text{m}$  spheres is approximately equal for both field  
 orientations. Nevertheless, the critical field magnitude  
 for the smaller 1  $\mu\text{m}$  diameter particles is significantly  
 lower for the perpendicular field. This result suggests  
 that a perpendicular field is the optimal configuration to  
 maximise the deviation of particles that are substantially  
 smaller than the critical diameter [33].



## V. CONCLUSIONS

575  
576  
577  
578  
579  
580  
581  
582  
583  
584  
585  
586

In conclusion, these numerical simulations have provided a comprehensive understanding of the factors that govern the low-frequency electrokinetic-induced sorting of particles inside a microfluidic DLD channel. We have demonstrated that the CPEO wall-particle interaction combined with EP oscillation fully explains the deflection induced by low-frequency electric fields, with the simulations matching the experimentally observed trends. Note that electrothermal flows have been neglected, given that this phenomenon occurs at higher electrolyte conductivities.

587  
588  
589  
590  
591

By establishing a link between the recently reported CPEO mechanism and the low-frequency electrokinetic separation of particles in DLD devices, our model consolidates previous experimental and numerical results, completing the theoretical framework for a full understand-

592  
593  
594  
595  
596  
597  
598  
599  
600  
601  
602

ing of the behaviour of electrokinetic-biased DLD particle separation systems. The implications of our findings are significant in the design and optimization of DLD devices for particle sorting and fractionation, when combined with electric fields, enabling particles significantly smaller than the critical diameter to be deflected and sorted. The simulations can be used to tailor the physical and electrical properties of the particles to achieve specific separation outcomes, and to optimize the post-array geometry, field frequency and conductivity of the solution to enhance separation efficiency.

## ACKNOWLEDGMENTS

P.G.S. and A.R. acknowledge Grant P20-00534 funded by "Consejería de Economía, Conocimiento, Empresas y Universidad (Junta de Andalucía)".

607  
608  
609  
610  
611  
612  
613  
614  
615  
616  
617  
618  
619  
620  
621  
622  
623  
624  
625  
626  
627  
628  
629  
630  
631  
632  
633  
634  
635  
636  
637  
638  
639  
640  
641  
642  
643  
644  
645

[1] H. Cho, J. Kim, H. Song, K. Y. Sohn, M. Jeon, and K.-H. Han, *Analyst* **143**, 2936 (2018).  
 [2] H. W. Hou, M. E. Warkiani, B. L. Khoo, Z. R. Li, R. A. Soo, D. S.-W. Tan, W.-T. Lim, J. Han, A. A. S. Bhagat, and C. T. Lim, *Scientific reports* **3**, 1259 (2013).  
 [3] P. Ohlsson, M. Evander, K. Petersson, L. Mellhammar, A. Lehmusvuori, U. Karhunen, M. Soikkeli, T. Seppa, E. Tuunainen, A. Spangar, et al., *Analytical chemistry* **88**, 9403 (2016).  
 [4] J. C. Contreras-Naranjo, H.-J. Wu, and V. M. Ugaz, *Lab on a Chip* **17**, 3558 (2017).  
 [5] K. Louterback, J. D'Silva, L. Liu, A. Wu, R. H. Austin, and J. C. Sturm, *AIP advances* **2**, 042107 (2012).  
 [6] B. H. Wunsch, J. T. Smith, S. M. Gifford, C. Wang, M. Brink, R. L. Bruce, R. H. Austin, G. Stolovitzky, and Y. Astier, *Nature nanotechnology* **11**, 936 (2016).  
 [7] J. McGrath, M. Jimenez, and H. Bridle, *Lab on a Chip* **14**, 4139 (2014).  
 [8] L. R. Huang, E. C. Cox, R. H. Austin, and J. C. Sturm, *Science* **304**, 987 (2004).  
 [9] J. P. Beech, P. Jönsson, and J. O. Tegenfeldt, *Lab on a Chip* **9**, 2698 (2009).  
 [10] B. D. Ho, J. P. Beech, and J. O. Tegenfeldt, *Micromachines* **11**, 1014 (2020).  
 [11] V. Calero, P. Garcia-Sanchez, C. Honrado, A. Ramos, and H. Morgan, *Lab on a Chip* **19**, 1386 (2019).  
 [12] V. Calero, P. Garcia-Sanchez, A. Ramos, and H. Morgan, *Journal of Chromatography A* p. 461151 (2020).  
 [13] L. Liang, Y. Ai, J. Zhu, S. Qian, and X. Xuan, *Journal of colloid and interface science* **347**, 142 (2010).  
 [14] L. Liang, S. Qian, and X. Xuan, *Journal of colloid and interface science* **350**, 377 (2010).  
 [15] R. Fernandez-Mateo, V. Calero, H. Morgan, P. Garcia-Sanchez, and A. Ramos, *Physical Review Letters* **128**, 074501 (2022).  
 [16] R. Fernández-Mateo, P. García-Sánchez, V. Calero, H. Morgan, and A. Ramos, *Journal of Fluid Mechanics* **924** (2021).  
 [17] V. Calero, R. Fernández-Mateo, H. Morgan, P. García-

Sánchez, and A. Ramos, *Physical Review Applied* **15**, 014047 (2021).  
 [18] J. Lyklema, *Fundamentals of Interface and Colloid Science* (Academic Press Limited, 1995).  
 [19] H. Morgan and N. G. Green, *AC Electrokinetics: colloids and nanoparticles*. (Research Studies Press Ltd., 2003).  
 [20] M. von Smoluchowski, *Bull. Akad. Sci. Cracovie.* **8**, 182 (1903).  
 [21] N. Gamayunov, V. Murtsovkin, and A. Dukhin, *Colloid J. USSR (Engl. Transl.);(United States)* **48** (1986).  
 [22] J. Happel and H. Brenner, *Low Reynolds number hydrodynamics: with special applications to particulate media*, vol. 1 (Springer Science & Business Media, 2012).  
 [23] E. Yariv, *Proceedings of the Royal Society A: Mathematical, Physical and Engineering Sciences* **465**, 709 (2009).  
 [24] J. R. Smart and D. T. Leighton Jr, *Physics of Fluids A: Fluid Dynamics* **3**, 21 (1991).  
 [25] S.-C. Kim, B. H. Wunsch, H. Hu, J. T. Smith, R. H. Austin, and G. Stolovitzky, *Proceedings of the National Academy of Sciences* **114**, E5034 (2017).  
 [26] J. E. Flores-Mena, P. García-Sánchez, and A. Ramos, *Micromachines* **14**, 23 (2022).  
 [27] R. V. Davalos, G. J. McGraw, T. I. Wallow, A. M. Morales, K. L. Krafcik, Y. Fintschenko, E. B. Cummings, and B. A. Simmons, *Analytical and bioanalytical chemistry* **390**, 847 (2008).  
 [28] M. Viefhues, S. Manchanda, T.-C. Chao, D. Anselmetti, J. Regtmeier, and A. Ros, *Analytical and bioanalytical chemistry* **401**, 2113 (2011).  
 [29] R. Fernández-Mateo, P. García-Sánchez, V. Calero, A. Ramos, and H. Morgan, *Electrophoresis* **43**, 1259 (2022).  
 [30] R. Fernández-Mateo, P. García-Sánchez, V. Calero, A. Ramos, and H. Morgan, *Electrophoresis* **43**, 1259–1262 (2022).  
 [31] V. Calero, P. Garcia-Sanchez, A. Ramos, and H. Morgan, *Biomicrofluidics* **13**, 054110 (2019).  
 [32] B. D. Ho, J. P. Beech, and J. O. Tegenfeldt, *Micromachines* **12** (2021).

685 [33] R. J. Gillams, V. Calero, R. Fernandez-Mateo, and  
686 H. Morgan, Lab on a Chip **22**, 3869 (2022).

Journal Pre-proof

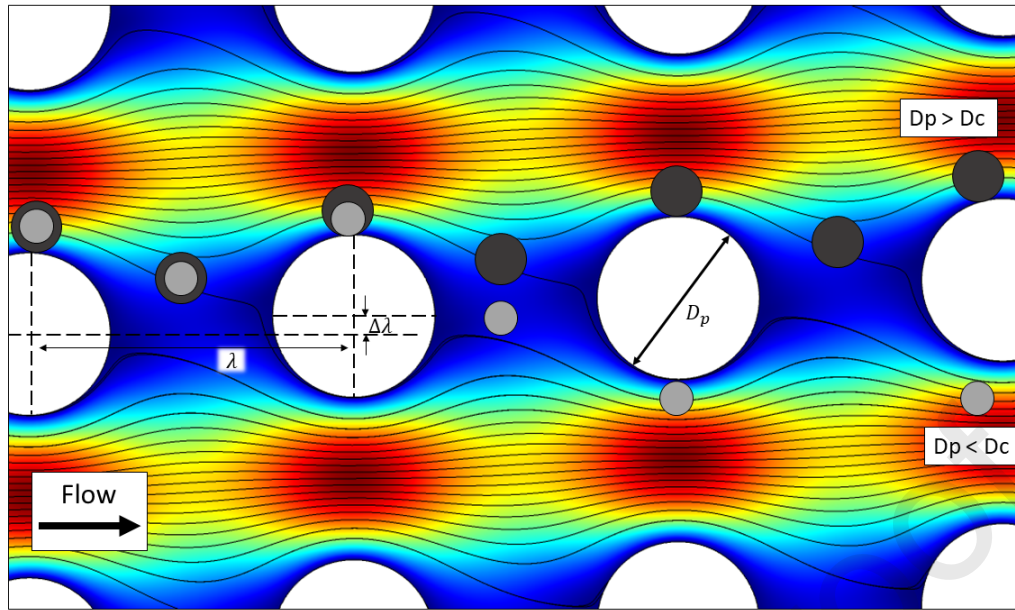


FIG. 1. Diagram representing a typical DLD cylindrical pillar array geometry. The passive size-based separation mechanism relies on the separatrix streamline which divides the flow passing above and below the following post. Particles bigger than a critical diameter  $D_c$  are displaced by the posts periodically while particles smaller follow the streamlines in an overall straight trajectory. The colour map represent the magnitude of the fluid velocity.

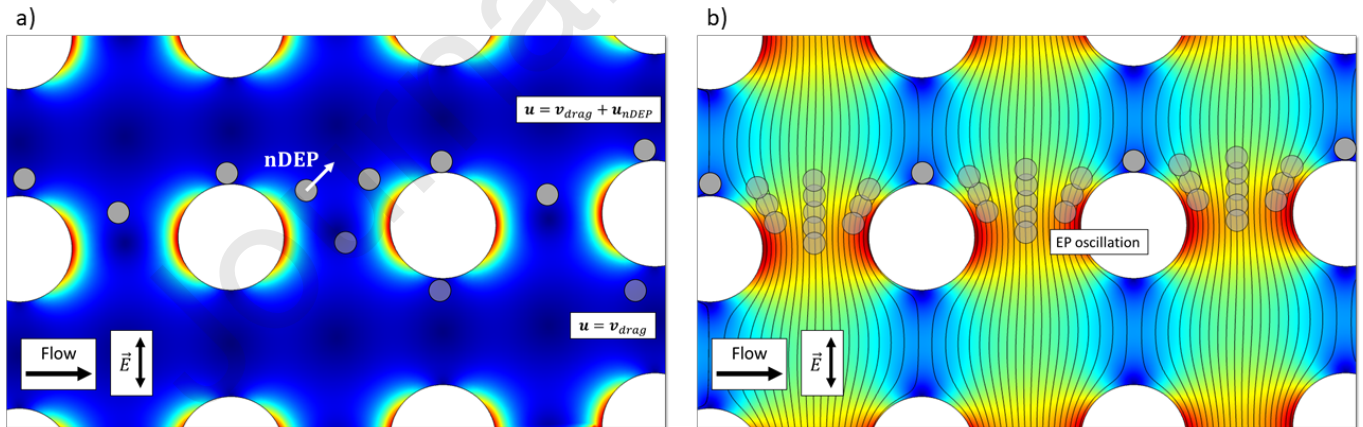


FIG. 2. Diagram of electrically tuned DLD separation. (a) Negative DEP induced separation - Colour map represents the intensity of the nDEP force. (b) Low frequency separation - Colour map represents the magnitude of the electric field.

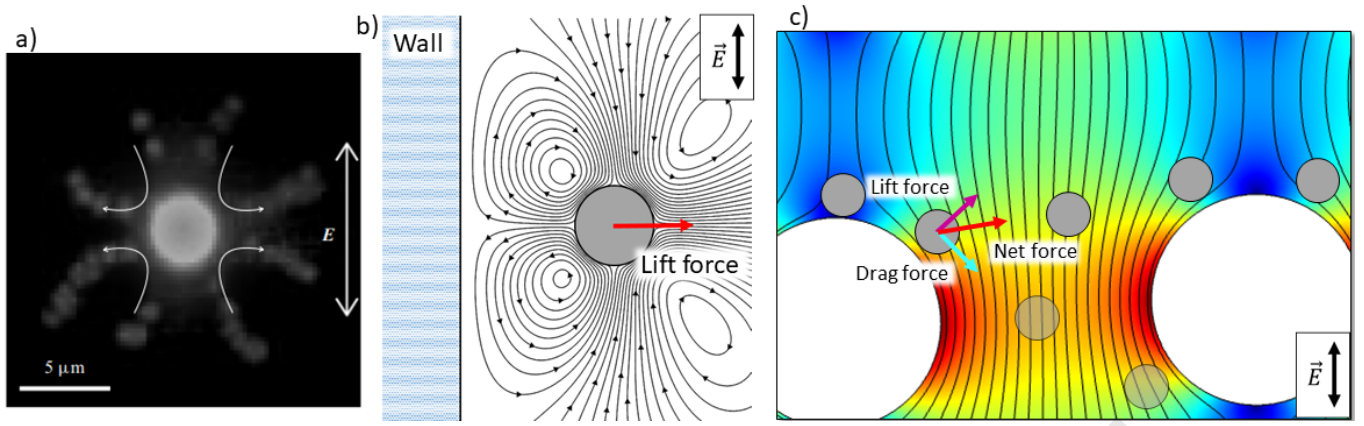


FIG. 3. Principles of CPEO assisted particle deviation in DLD arrays. (a) Experimentally observed CPEO flows around a  $3 \mu\text{m}$  carboxylate particle ( $f = 282 \text{ Hz}$  and  $E = 80 \text{ kV/m}$ ) using  $500 \text{ nm}$  fluorescent spheres as flow tracers. Reproduced from Fernández-Mateo *et al.* [16] (with permission from Cambridge University Press 2021). (b) Particle repulsion from a flat wall induced by CPEO flows around the particles. (c) Deviation inside DLD post array induced by CPEO wall repulsion - Colour map represents the magnitude of the electric field.

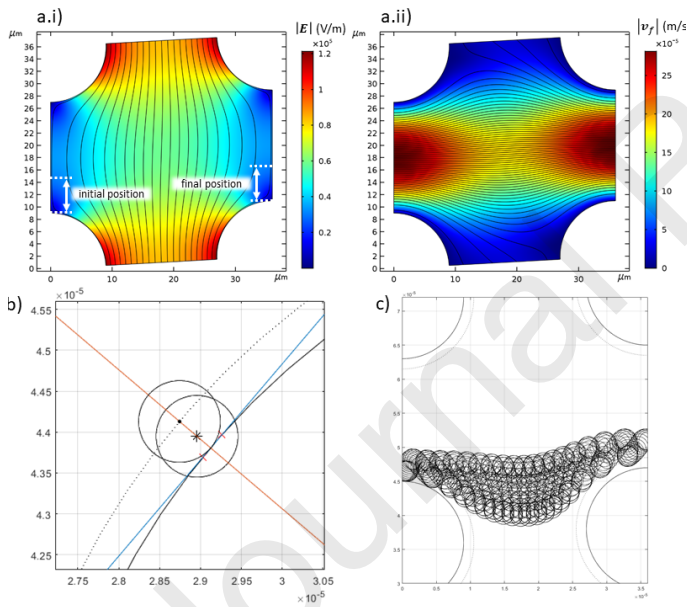


FIG. 4. (a.i) Electric field distribution calculated in the DLD unit cell, marking the initial and final position of the particles. (a.ii) Fluid flow profile inside the DLD unit cell. (b) Hard wall inelastic-collision correction. The initial position (marked with an asterisk in the particle centre) is corrected for the distance of the overlap between particle and post, to the position marked with a dot in the particle centre. (c) Example trajectory of the deviation of a  $3 \mu\text{m}$  particle at low frequencies induced by CPEO and EP oscillations.

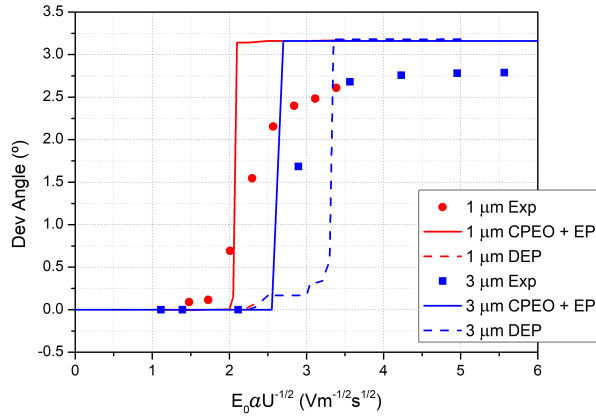


FIG. 5. Comparison of experimental data for 1  $\mu\text{m}$  and 3  $\mu\text{m}$  particles with simulation results: (electrolyte conductivity of 2.8 mS/m and field frequency of 50 Hz) at low frequencies including EP oscillation and CPEO wall interaction (solid lines) and high frequencies with nDEP (dashed lines). Note that the simulation results for the high-frequency deviation of 1  $\mu\text{m}$  and 3  $\mu\text{m}$  collapse and overlap.

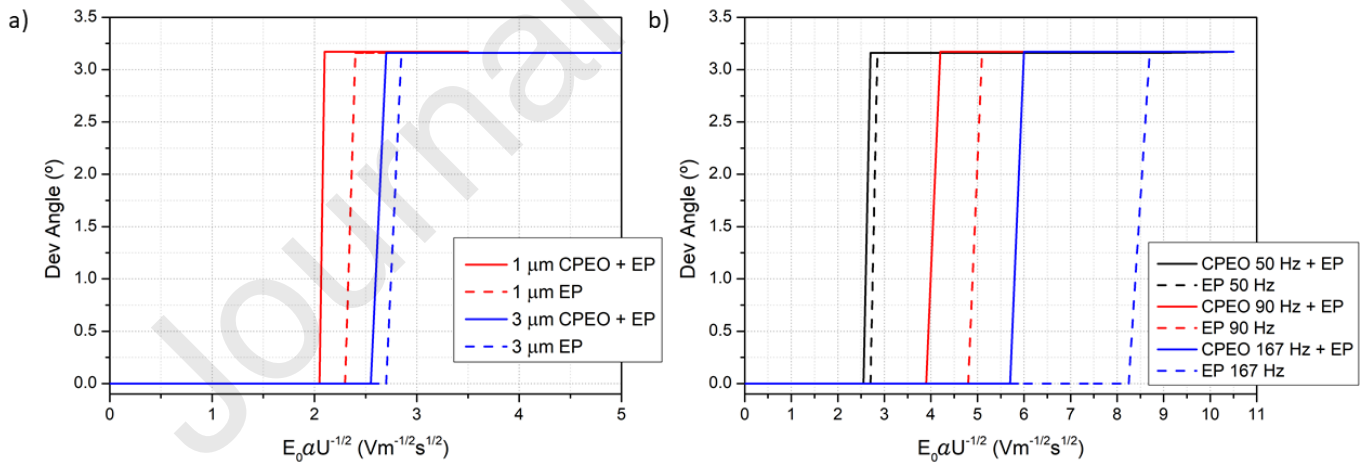


FIG. 6. Comparison of the deviation induced by EP oscillation only and EP oscillation combined with CPEO induced deviation. (a) Two different particle sizes at 50 Hz. (b) 3  $\mu\text{m}$  diameter particles at different field frequencies.

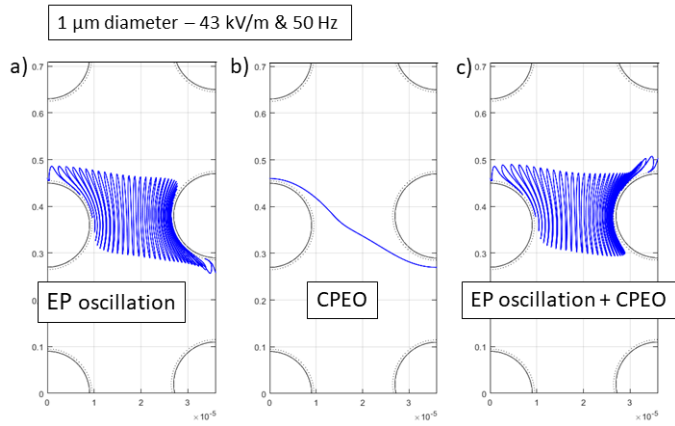


FIG. 7. Example of simulated trajectories of 1  $\mu\text{m}$  diameter particle inside DLD devices with a low (50 Hz) frequency electric field perpendicular to the fluid flow. (a) Contribution only from electrophoretic oscillation. (b) Only CPEO contribution. (c) Combination of CPEO and EP oscillation.

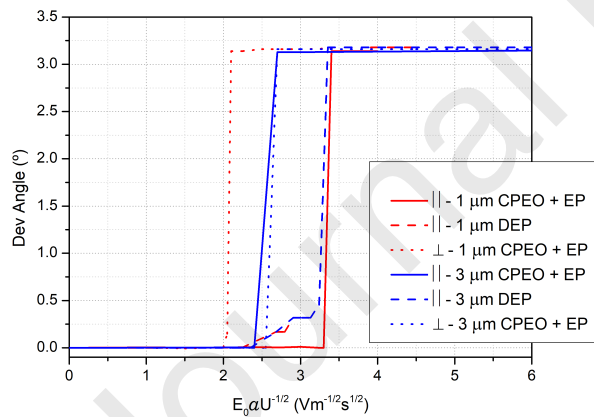


FIG. 8. Comparison between nDEP and low-frequency induced deviation for an electric field applied parallel to the fluid flow ( $\parallel$ ) and the low-frequency deviation induced by an electric field perpendicular to the fluid flow ( $\perp$ ). Note that, as in Figure 5, the simulation results for the high-frequency deviation of 1  $\mu\text{m}$  and 3  $\mu\text{m}$  overlap.

**Declaration of interests**

The authors declare that they have no known competing financial interests or personal relationships that could have appeared to influence the work reported in this paper.

The authors declare the following financial interests/personal relationships which may be considered as potential competing interests:

Journal Pre-proof

CRediT authorship contribution statement

**Víctor Calero:** Conceptualization, Methodology, Software, Validation, Formal analysis, Investigation, Data curation, Writing - original draft, Visualization.

**Raúl Fernández-Mateo:** Methodology, Software, Validation, Formal analysis, Investigation, Data curation, Writing - review & editing.

**Hywel Morgan:** Validation, Formal analysis, Writing - review & editing, Funding acquisition.

**Pablo García-Sánchez:** Conceptualization, Methodology, Software, Validation, Formal analysis, Writing - review & editing, Supervision.

**Antonio Ramos:** Conceptualization, Methodology, Validation, Formal analysis, Writing - review & editing, Supervision, Funding acquisition.

Journal Pre-proof